EDGE ARTICLE

Check for updates

A designed second-sphere hydrogen-bond interaction that critically influences the O−O bond activation for heterolytic cleavage in ferric iron–porphyrin complexes†

Sarmistha Bhunia, [a] Atanu Rana, [a] Somdatta Ghosh Dey, *[a] Anabella Ivancich *[b] and Abhishek Dey *[a]

Heme hydroperoxidases catalyze the oxidation of substrates by H_2O_2. The catalytic cycle involves the formation of a highly oxidizing species known as Compound I, resulting from the two-electron oxidation of the ferric heme in the active site of the resting enzyme. This high-valent intermediate is formed upon facile heterolysis of the O−O bond in the initial Fe^{III}−OOH complex. Heterolysis is assisted by the histidine and arginine residues present in the heme distal cavity. This chemistry has not been successfully modeled in synthetic systems up to now. In this work, we have used a series of iron(III) porphyrin complexes (Fe^{III}L2(Br), Fe^{III}L3(Br) and Fe^{III}MPh(Br)) with covalently attached pendent basic groups (pyridine and primary amine) mimicking the histidine and arginine residues in the distal-pocket of natural heme enzymes. The presence of pendent basic groups, capable of 2nd sphere hydrogen bonding interactions, leads to almost 1000-fold enhancement in the rate of Compound I formation from peracids relative to analogous complexes without these residues. The short-lived Compound I intermediate formed at cryogenic temperatures could be detected using UV-vis electronic absorption spectroscopy and also trapped to be unequivocally identified by 9 GHz EPR spectroscopy at 4 K. The broad (2000 G) and axial EPR spectrum of an exchange-coupled oxoferryl-porphyrin radical species, [Fe^{IV}=O Por$^{•+}$] with $g_\perp^{eff} = 3.80$ and $g_\parallel^{eff} = 1.99$, was observed upon a reaction of the Fe^{III}L3(Br) porphyrin complex with *m*-CPBA. The characterization of the reactivity of the Fe^{III} porphyrin complexes with a substrate in the presence of an oxidant like *m*-CPBA by UV-vis electronic absorption spectroscopy showed that they are capable of oxidizing two equivalents of inorganic and organic substrate(s) like ferrocene, 2,4,6-tritertiary butyl phenol and *o*-phenylenediamine. These oxidations are catalytic with a turnover number (TON) as high as 350. Density Functional Theory (DFT) calculations show that the mechanism of O−O bond activation by 2nd sphere hydrogen bonding interaction from these pendent basic groups, which are protonated by a peracid, involves polarization of the O−O σ-bond, leading to lowering of the O−O σ*-orbital allowing enhanced back bonding from the iron center. These results demonstrate how inclusion of 2nd sphere hydrogen bonding interaction can play a critical role in O−O bond heterolysis.

Introduction

Factors that can affect heterolytic O–O bond cleavage of metal peroxide species are of great contemporary interest.[1,2] Heterolysis of metal peroxides generates high-valent metal oxo species which are very reactive and have been demonstrated to be able to catalyze oxidation of inert organic Compounds, a process that is highly relevant to the chemistry community.[3–7] The

inspiration for such chemistry is derived from naturally occurring heme metalloenzymes (monofunctional peroxidases,[8] catalases,[9] bifunctional catalase-peroxidases (KatGs),[10] cyt P450 monooxygenases[11] and P450 peroxygenases[12]) where detailed biochemical experiments heralded the presence of 1st and 2nd coordination sphere residues in the heme active site that are essential for the generation of high-valent catalytic intermediates. The resting state of peroxidases, peroxygenases and catalases is the ferric oxidation state of the heme iron and a catalytically-competent high-valent intermediate [Fe^{IV}=O Por$^{•+}$], Compound I, is formed by the reaction with hydrogen peroxide or alternative two-electron oxidants. Upon reaction with substrates, the one-electron reduction of Compound I results in the formation of the Fe^{IV}=O species known as

[a] Department of Inorganic Chemistry, Indian Association for the Cultivation of Science, Kolkata, 700032, India. E-mail: icad@iacs.res.in

[b] CNRS, Aix-Marseille Univ, Laboratoire de Bioénergétique et Ingénierie des Protéines (UMR 7281), IMM FR3479, Marseille, France. E-mail: aivancich@imm.cnrs.fr

† Electronic supplementary information (ESI) available. See DOI: 10.1039/c9sc04388h

Compound **II**, which undergoes further one electron reduction and regains back the resting ferric state.[13] The Compound **I** intermediate is the strongest oxidant in the catalytic cycle of peroxidases which are involved in several activities like biosynthesis of hormones (cycloperoxidases), defense against pathogens (myeloperoxidase and horseradish peroxidase) and regulating cellular oxidative stress (CcP and GSH peroxidase).[14,15] The oxidizing ability of high valent intermediates makes them valuable to the chemical industry as they can catalyze difficult chemical oxidations relevant to synthesis of fine chemicals, waste water decontamination of toxic phenol and polymerization.[16,17] The ferric hydroperoxide (Fe^{III}–OOH) intermediate, known as Compound **0**,[18,19] is the very short-lived species preceding the formation of Compound **I** in all hydroperoxidases[20,21] A histidine residue is involved in the protonation of Compound **0** in the active site of peroxidases.[22–24] Histidine acts as a base initially deprotonating the proximal oxygen atom of hydroperoxide bound to the heme iron, and then transfers the proton to a distal oxygen atom as an acid catalyst to facilitate the heterolytic O–O bond cleavage and water release, assisted by an arginine residue, leaving the oxygen atom bound to the iron (Fig. 1).[20,24–27]

The arginine residue, being positively charged at neutral pHs, likely helps in polarization of the O–O bond and promotes heterolysis as its mutation leads to a two orders of magnitude reduction in the rates.[28] This combined role of histidine and arginine residues in the heme distal side exerts a "Pull-effect" and results in facile heterolytic cleavage of the O–O bond.[20,24,26,29] Such a "Pull effect" is also exhibited by other peroxidases with a similar distal acid-base residue.[30–32] The arginine residue forms a hydrogen bond with the ferryl oxygen atom of Compound **I** and thus may stabilize the high valent reactive intermediates.[28] The arginine residue enhances the binding of a substrate to the peroxidase active site as its mutation increases K_M of the substrate.[33–35] Peroxidases such as HRP show minimal heme degradation during catalysis, mostly occurring in the presence of very high molar excess of the oxidant.[36,37]

Over the last several decades, several synthetic systems were designed for the investigation of the "Push–Pull" effect and the formation of Compound **I** was examined using various oxidants.[38–41] Watanabe and coworkers monitored the formation of Compound **I** in an organic medium with peracids in a series of synthetic iron-porphyrins by varying the substituents in their *meso* phenyl rings and also using substituted axial imidazole ligands.[42] Groves and coworkers demonstrated that the nature of the bond cleavage process can be controlled by changing the polarity of solvents in some systems.[43,44] Fujii and coworkers examined the spin coupling interaction between the ferryl iron and the porphyrin π-cation radical using EPR spectroscopy to probe the a_{1u}/a_{2u} character of the high-valent intermediates in several iron porphyrins with different substituents in *meso* phenyl rings and β-pyrroles.[45] Nocera and co-workers introduced hanging carboxylic acid residues to impose 2nd sphere interactions with reactive intermediate mimicking the distal residues in the protein active site which promote heterolytic bond fission.[46,47] Unfortunately, the reported rates for O–O bond heterolysis did not indicate a substantial role of the pendent carboxylic acids.[46] In a very recent work, incorporation of a pendent amine group into the 2nd coordination sphere of a non heme iron complex has been reported to form selectively the Fe^{IV}=O intermediate *via* heterolytic O–O bond cleavage with a lower activation energy barrier by the reaction of the non-heme Fe(II) complex with H_2O_2.[5]

To date, the role of the histidine residue as an acid-base catalyst in the distal site of peroxidases remains to be successfully modeled in any synthetic heme-based model system. Peroxidases generally oxidize organic phenols and aromatic amines using an outer sphere electron transfer and oxidation of substrates like epoxidation and sulfoxidation, traditionally performed by monooxygenases, is reported.[48–53] So far, molecular mimics of the Compound **I** intermediate of peroxidases are reported to catalyze epoxidation and sulfoxidation with a low turnover number or yield.[47,54,55] Yet, catalytic oxidation of phenols and amines, the typical substrates for peroxidases with a significant turnover number, has not been achieved.[56–58] This is particularly important as the hydroperoxidase activity is a key technology for degradation of organic contaminants in water. Thus, facile generation of a synthetic reactive intermediate mimicking Compound **I** to be used for catalytic transformations and retarding its self-degradation is of interest to a broad community of chemists. Recently, mononuclear (ferric) iron porphyrins with pendent basic groups were reported (Fig. 2B
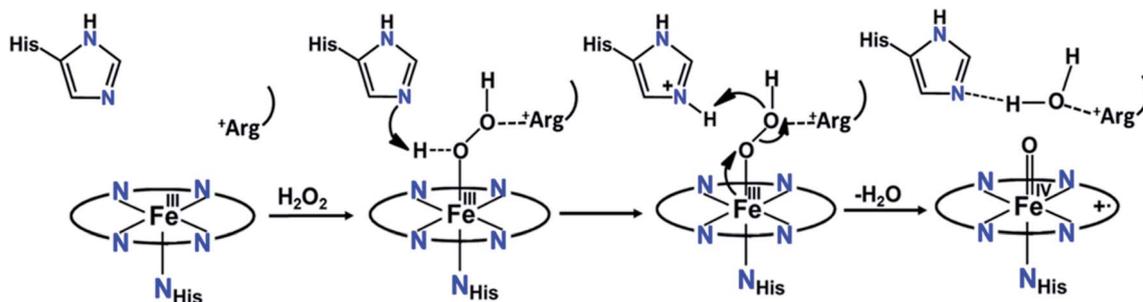

Fig. 1 Mechanism for the formation of the Compound I intermediate in peroxidases, involving the His and Arg residues of the heme distal side.[15,27,28]

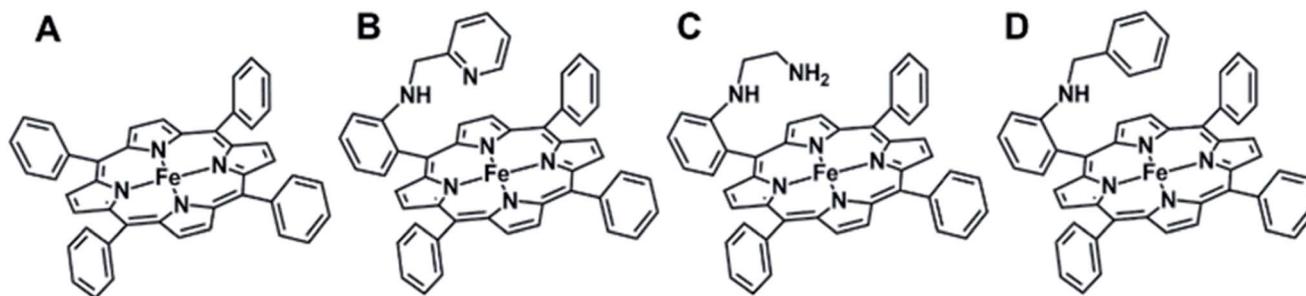Fig. 2 Molecular structures of iron–porphyrin complexes used in this study: (A) Fe^{III}TPP, (B) Fe^{III}L2, (C) Fe^{III}L3 and (D) Fe^{III}MPh.

and C) which could reduce oxygen to water with greater than 95% selectivity at pH 7 with rates >10^7 M^{-1} s^{-1}.[59] The origin of such high reactivity and much desired selectivity in simple mononuclear iron porphyrin was proposed to originate from specific proton transfer to the distal oxygen, akin to peroxidases, of a putative ferric hydroperoxide species from the pendent basic groups which remains protonated at pH 7. These proposals were supported by DFT calculations.[59]

In this work, we have used a series of ferric iron porphyrin complexes with pendent basic groups covalently attached to the amine group of the *meso*-phenyl ring (see Fig. 2) in the tetraphenylporphyrin architecture, in order to investigate the rates of O–O bond heterolysis and to characterize the ensuing intermediates formed. Compound **I** is detected upon oxidation of these ferric iron porphyrin complexes with a peracid (*m*-chloroperbenzoic acid), as clearly shown by the stopped-flow kinetics and EPR spectroscopic characterization. Pyridine and amine, designed as pendent groups emulating the distal His residue in natural peroxidases (see Fig. 1), translocate protons from the proximal to distal oxygen atom of bound *m*-chloroperbenzoic acid to facilitate the heterolytic cleavage pathway with much higher rates than the benzyl analogue (Fig. 2D, Fe^{III}MPh(Br)), a structurally analogous iron porphyrin without base, and also than any previously reported synthetic porphyrins thus with rates comparable to natural peroxidases. The results also suggest that the self-degradation of the Fe^{III} porphyrin catalyst was prevented, most likely by the hydrogen bonding interaction of the pendent base with the Fe^{IV}=O center of Compound **I**, thus allowing these synthetic hemes to efficiently catalyze the oxidation of organic and inorganic substrates using peracids. Density Functional Theory (DFT) calculations support the experimentally observed activation of a bound peroxide by pendent bases and help in developing a molecular orbital theory rationale of the elusive "pull effect".

Results and discussion

The formation of high valent iron-oxo intermediates was examined for four iron(III) porphyrin model complexes (Fig. 2) *e.g.*, Fe^{III}L2(Br) and Fe^{III}L3(Br) each containing a distinct pendent (basic) residue pyridine and aliphatic amine, respectively, Fe^{III}MPh(Br) containing a mono benzyl group without additional basic residue and simple mononuclear iron

porphyrin without any second sphere residue (Fe^{III}TPP(Br)) (Fig. 2). *m*-CPBA was used as an oxidant. The pK_a values of the pendent pyridine and amine groups in Fe^{III}L2(Br) (Fig. 2A) and Fe^{III}L3(Br) (Fig. 2B) complexes were determined to be 12.33 and 16.90, respectively, in CH$_3$CN.[60] The reactions were monitored at sub-zero temperatures using a stopped-flow UV-vis electronic absorption spectrometer.

Upon reaction of Fe^{III}L2(Br) with *m*-CPBA in dichloromethane (DCM) at −30 °C, the electronic absorption spectrum of the ferric state showed a decrease in the intensity of the Soret (417 nm) and charge transfer bands at 510 nm, 594 nm and 695 nm. In addition, a new and rather broad band centered at *ca.* 705 nm was also observed (Fig. 3A). Similar changes were observed for the Fe^{III}L3(Br) complex under the same conditions where a broad band appeared at *ca.* 726 nm (Fig. 3B). In the case of the Fe^{III}MPh(Br) complex, where no basic residue is present, a new broad band at *ca.* 705 nm (Fig. 3C) was observed. The broad charge transfer band at ~700 nm is consistent with the formation of the iron(IV)-oxo porphyrin cation radical intermediate, Compound **I**, previously reported in synthetic model complexes and in enzyme systems.[43,46,61–65]

The formation of the 705 nm band of Fe^{III}L2(Br) maximizes within 5 s (Fig. 3D, green trace & S1A,† red trace). The species is quite stable at −30 °C and disappears in *ca.* 5 minutes (Fig. S4B,† blue trace). However, the formation of this band takes much longer time, *i.e.* around 1 min, in the case of Fe^{III}MPh(Br) (Fig. 3D & S1C,† violet trace). The absorbance at the 726 nm band for Fe^{III}L3(Br) maximizes within 500 ms (Fig. S1B,† green trace) and decays by 10 s (Fig. 3D, red trace & S4A,† green trace) at −30 °C. The rate constants for the formation of Compound **I** are 21.67 ± 1 s^{-1}, 67.6 ± 2 s^{-1} and $(8.5 ± 1) × 10^{-2}$ s^{-1} for Fe^{III}L2(Br), Fe^{III}L3(Br) and Fe^{III}MPh(Br), respectively (Fig. 4) at −30 °C (*i.e.* 243 K). A more than two orders of magnitude faster O–O bond heterolysis in Fe^{III}L2 and Fe^{III}L3 with respect to Fe^{III}MPh provides definitive proof of the advantage of the pendent nitrogenous bases during heterolytic cleavage. The first order rate constants for these two complexes are even much higher than those for previously reported model complexes (Table 1). The rate constants for the decay of these bands are $(3.2 ± 0.5) × 10^{-1}$ s^{-1} and $(5 ± 0.7) × 10^{-3}$ s^{-1} for Fe^{III}L2(Br) and Fe^{III}L3(Br), respectively, obtained from the first order exponential fits to the absorbance *vs.* time traces (Fig. 4). The Compound **I** intermediate for both of these complexes is
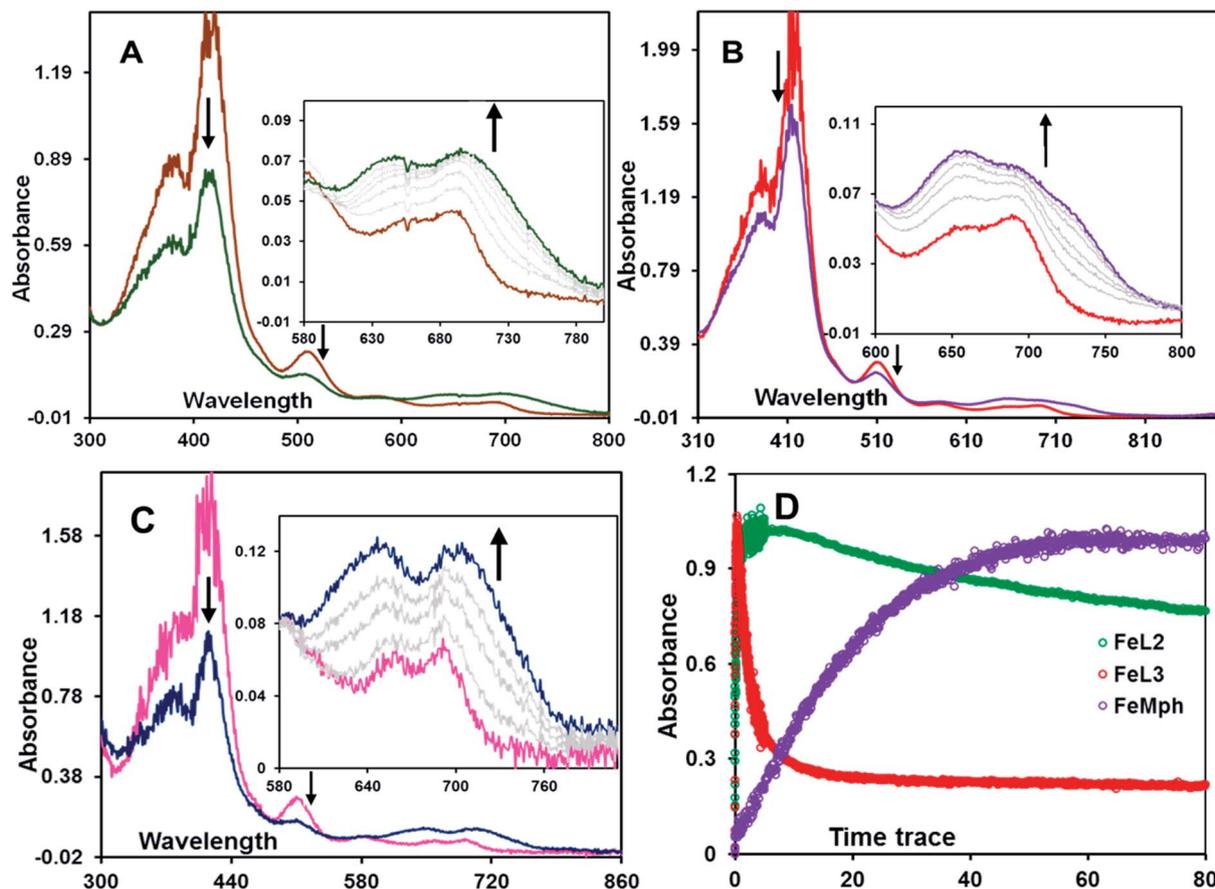
Fig. 3 Stopped-flow absorption spectral changes after the reaction of 50 μM complexes (A) $Fe^{III}L2(Br)$, (B) $Fe^{III}L3(Br)$ and (C) $Fe^{III}MPh(Br)$ with 200 μM m-CPBA in dichloromethane at −30 °C. In (A) brown solid line: resting $Fe^{III}L2(Br)$ at the beginning of the reaction, green line: the intermediate formed at 5 s corresponding to $[Fe^{IV}=O\ Por^{•+}]L2$; in (B) red line: resting $Fe^{III}L3(Br)$ at the beginning of the reaction, violet line: the intermediate formed at 500 ms corresponding to $[Fe^{IV}=O\ Por^{•+}]L3$; in (C) pink line: resting $Fe^{III}MPh(Br)$ at the beginning of the reaction, blue line: the intermediate formed after 1 minute corresponding to $[Fe^{IV}=O\ Por^{•+}]MPh$, grey lines: the conversion as a function of time from resting iron(III)-porphyrins to intermediate species, after addition of m-CPBA. (D) Red circles: time trace of $Fe^{III}L3$ at 726 nm, green circles: time trace of $Fe^{III}L2$ at 705 nm and violet circles: time trace of $Fe^{III}MPh$ at 705 nm.

converted to the corresponding Compound **II** ($Fe^{IV}=O$) species as indicated by the characteristic bands at 650 nm and 657 nm for $Fe^{III}L2(Br)$ and $Fe^{III}L3(Br)$, respectively, which is stable for several minutes at −30 °C (Fig. S3†). Note that the formation and decay of Compound **I** can be fit using a kinetic model for consecutive reactions (Fig. S4†) suggesting that the disproportionation of Compound **II** to form Compound **I** and ferric species is not observed here as has been reported for non-heme systems.[66–68]

The reaction of m-CPBA with $Fe^{III}TPP(Br)$ under identical conditions did not show the formation of Compound **I**, rather it showed a very slow formation of isoporphyrin, a species isoelectronic with Compound **I** and an intermediate in heme degradation of the heme oxygenase cycle that has characteristic bands at 810 nm and 900 nm (Fig. 5A, red trace and Fig. S2†) suggesting the decay pathway of the porphyrin macrocycle of $Fe^{III}TPP(Br)$ consistent with previous literature (Scheme S1†).[36,62,69] Alternatively, the $Fe^{III}L2(Br)$ and $Fe^{III}L3(Br)$ complexes form their high valent oxo species and decay to their resting ferric state in their reaction with mCPBA in contrast to

$Fe^{III}TPP(Br)$ (Fig. 5A). Note that minor and sluggish formation of isoporphyrin is detected in $Fe^{III}L2(Br)$, $Fe^{III}L3(Br)$ and $Fe^{III}MPh(Br)$ as indicated by the absorption spectra and time traces of 800 nm and 900 nm bands (Fig. 5A and B; S1A–S1C†) and is likely due to competitive binding of m-CPBA at the open site of the porphyrin, which logically follows a $Fe^{III}TPP$-like reactivity (Fig. S2†). Overall, it is clear that the pendent basic groups avoid degradation of the heme upon its reaction with peracids.

The rates of Compound **I** formation from ferric porphyrins *via* heterolysis of the O–O bond of bound peracid (m-CPBA) are obtained at −30 °C. Since the kinetics for formation of the Compound **I** have been obtained at different temperatures than previously reported metalloporphyrin systems, a direct comparison of the rate constants is not possible (Fig. 6, Table 1). The activation energies ($\Delta G^{\neq}$) for O–O bond heterolysis of $Fe^{III}L2$ and $Fe^{III}L3$ are obtained from the observed rates using the Eyring equation and compared to those calculated for different model iron porphyrins (Table 1) from their reported rates.[42,46] The lowest energy barrier attained is 12.78 kcal mol^{-1}
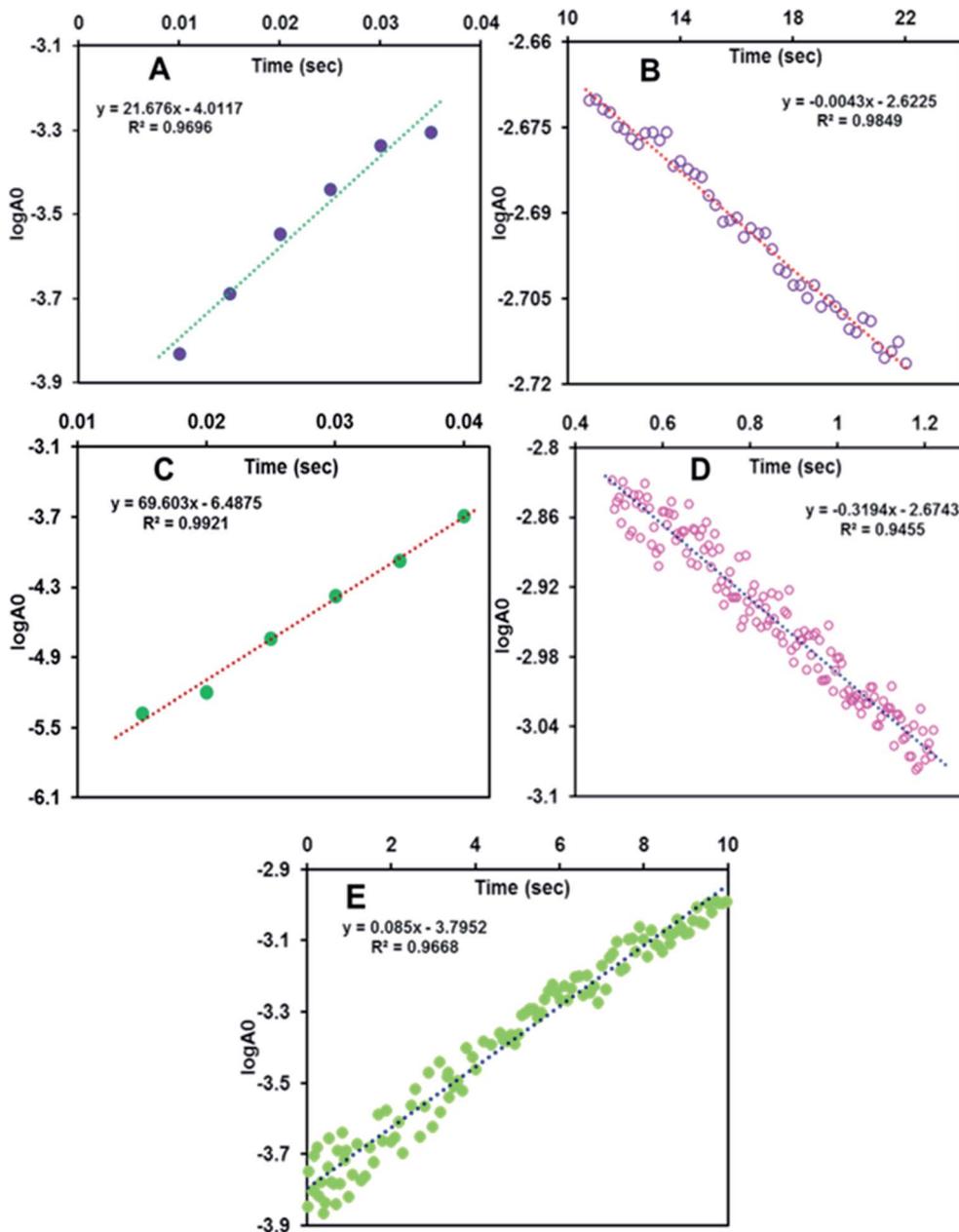
Fig. 4 Linear fit of initial log A_0 vs. time trace: reaction of $Fe^{III}L2(Br)$ (50 μM) with 4 eq. m-CPBA (100 μM) in dichloromethane at −30 °C leads to the formation of the Compound I intermediate (λ_{max} = 710 nm) represented by blue circles (A) and decay of the Compound I intermediate represented by purple circles (B). The first order rate constants obtained from the slopes of the log A_0 vs. t plot for the formation and decay of Compound I are 21.67 s^{-1} and 0.004 s^{-1}, respectively. Reaction of $Fe^{III}L3(Br)$ (50 μM) with 8 eq. m-CPBA (200 μM) in dichloromethane at −30 °C leads to the formation of the Compound I intermediate (λ_{max} = 726 nm) represented by green circles (C) and decay of the Compound I intermediate indicated by pink circles (D). The first order rate constants obtained from the slopes of the log A_0 vs. t plot for the formation and decay are 69.60 s^{-1} and 0.32 s^{-1}, respectively. (E) Reaction of $Fe^{III}Mph(Br)$ (50 μM) with 8 eq. m-CPBA (200 μM) in dichloromethane at −30 °C leads to the formation of the Compound I intermediate (λ_{max} = 710 nm) represented by green circles. The first order rate constant (obtained from the slope of log A_0 vs. time plot) for Compound I formation is 0.085 s^{-1}.

for complex **6a** (Fig. 6) which has the most electron rich porphyrin ring among all of the synthetic models reported to date. The presence of a large number of electron donating methoxy substituents in **6a** makes it facile to undergo faster heterolytic O–O bond cleavage than any other *meso* substituted porphyrins as reported by Watanabe *et al.*[42] The $\Delta G^{\#}$ values of

$Fe^{III}L2(Br)$, $Fe^{III}L3(Br)$ and $Fe^{III}MPh(Br)$ for O–O bond heterolysis are calculated be 12.72 ± 0.02 kcal mol^{-1}, 12.15 ± 0.01 kcal mol^{-1} and 15.08 ± 0.05 kcal mol^{-1}, respectively. The activation energies of pendent base containing models match well with those of the earlier reported models (**6a** and **6b**, Table 1). We have derived two other activation parameters *i.e.*

Table 1 The rate of O−O heterolysis and the corresponding activation parameters[a]

Catalyst	$k_{heterolysis}$ (s^{-1})	Temperature	$\Delta G^{\neq}$ (kcal mol^{-1})	Ref.
6a	16.6×10^{-3}	$-80\ ^\circ$C	12.78	41
6b	4×10^{-3}	$-80\ ^\circ$C	13.33	41
6d	3.94×10^{-3}	$-40\ ^\circ$C	16.19	41
6e	0.5×10^{-4}	$-80\ ^\circ$C	14.14	41
Fe^{III}TMP	$(6.5 \pm 1) \times 10^{-3}$	$-40\ ^\circ$C	15.96 ± 0.1	45
Fe^{III}(HPX-CO$_2$H)	$(6 \pm 3) \times 10^{-3}$	$-40\ ^\circ$C	15.99 ± 0.2	45
Fe^{III}(HPX-CO$_2$Me)	$(1 \pm 0.2) \times 10^{-2}$	$-40\ ^\circ$C	15.76 ± 0.1	45
Fe^{III}L2	21.67 ± 1	$-30\ ^\circ$C	12.72 ± 0.02	This work
Fe^{III}L3	69.6 ± 2	$-30\ ^\circ$C	12.15 ± 0.01	This work
Fe^{III}MPh	$(8.5 \pm 1) \times 10^{-2}$	$-30\ ^\circ$C	15.08 ± 0.05	This work
HRP	200–500 s^{-1}	25 $^\circ$C	13–14	53 and 70
H42A/H42V	$(5-50) \times 10^{-4}$	25 $^\circ$C	21 ± 1	71 and 73

[a] The molecular structures (**6a**, **6b**, **6d** and **6e**) corresponding to ref. 41 are given in Fig. 6. Here, *meta*-chloroperbenzoic acid is used as an oxidant for all the catalysts except for ref. 53, 71 and 73 (where hydrogen peroxide is the oxidant).

$\Delta H^{\#}$ (2.34 ± 0.2 kcal mol^{-1}) and $\Delta S^{\#}$ (−44.60 ± 1 cal mol^{-1} K^{-1}) from the linear Arrhenius plot of the temperature dependent kinetic study for Compound **I** formation of Fe^{III}L2(Br). A remarkably low enthalpic barrier and large negative entropy of activation also support the facile O−O bond cleavage step. $\Delta G^{\#}$ (13.03 ± 0.3 kcal mol^{-1}) is also determined from kinetics at different temperatures from the sum of $\Delta H^{\#}$ and $\Delta S^{\#}$ which is in good agreement with that obtained directly from the first order rate constants using the Eyring equation (details in the ESI†). It is important to note that $\Delta G^{\#}$ for O−O bond heterolysis is 3–4 kcal mol^{-1} lower in Fe^{III}L2 and Fe^{III}L3 relative to structurally analogous Fe^{III}MPh, Fe^{III}TMP and iron-hangman porphyrins which have pendent carboxylic acid/ester groups (Table 1) directly establishing the efficacy of pendent basic groups in the enhancement of heterolytic O−O bond cleavage rates. Additionally, a three times faster rate and 0.5 kcal mol^{-1} lower $\Delta G^{\#}$ of Fe^{III}L3(Br) with an aliphatic amine (pk_a ∼ 16.9 in CH$_3$CN) than those of Fe^{III}L2(Br) with a pyridine group (pk_a ∼ 12.33 in CH$_3$CN) suggest that the O−O bond heterolysis is favored by pendent amine groups having higher basicity than the peracid. Therefore, these residues can easily act as efficient acid-base catalysts and are capable of deprotonating the distal oxygen

atom of bound peracid and transferring the proton to a distal oxygen atom that is necessary for heterolysis. The rate of Compound **I** formation from *m*-CPBA in native HRP is 200–500 s^{-1} and two histidine mutants of HRP; H42A and H42V show 10^5 to 10^6 order lowering of the rate *i.e.* $(5-50) \times 10^{-4}$ s^{-1} at room temperature.[53,70,71] The corresponding activation energy barrier for HRP (∼13–14 kcal mol^{-1}) is much lower than the histidine mutants (21 ± 1 kcal mol^{-1}) and comparable to that achieved in these synthetic models Fe^{III}L2(Br) and Fe^{III}L3(Br). Thus, the "pull effect" in peroxidases is successfully mimicked in synthetic models including pendent basic groups (analogous to the histidine residue) in the 2nd sphere of the iron porphyrin. Note that, mutation of the His42 residue in HRP leads to several orders of magnitude decrease in the rate of Compound **I** formation *via* O−O bond heterolysis,[27,72,73] which is reasonably captured in two orders of magnitude reduction in the rate of Compound **I** formation in the FeMPh relative to FeL2 and FeL3.

Identification of the high-valent intermediates by EPR spectroscopy

To further identify and characterize the catalytically-relevant high-valent intermediates (Compound **I** and Compound **II**)
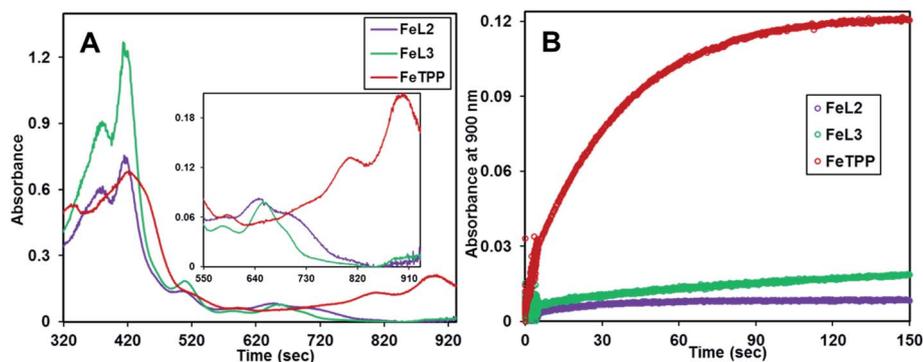

Fig. 5 Rapid-scan electronic absorption spectra of the reaction of iron porphyrin complexes (50 μM) with 8 equivalent of *meta*-chloroperbenzoic acid (*m*-CPBA, 200 μM) in dichloromethane followed at −30 $^\circ$C. (A) Selected overlay spectra representing the intermediate species formed after 50 s of the reaction, (B) overlay of the time traces at the 900 nm band with the formation of isoporphyrin species (λ_{max} = 900 nm) for these three complexes (Fe^{III}TPP(Br) (red line), Fe^{III}L2(Br) (violet line) and Fe^{III}L3(Br) (green line)).
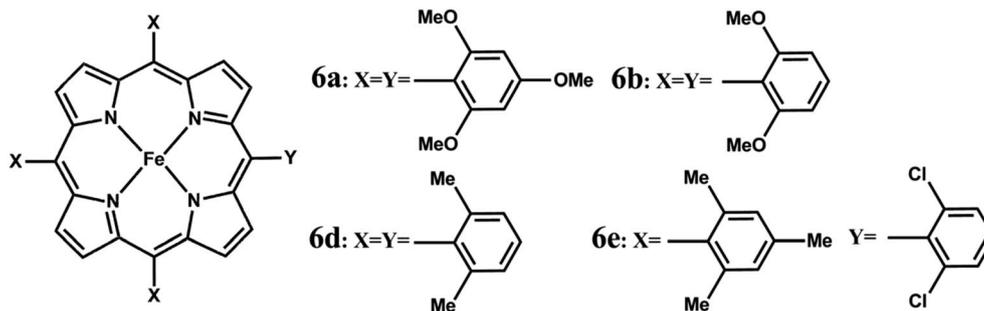
Fig. 6 Structures of model iron-porphyrins referred to in Table 1.

proposed from the spectral changes in the electronic absorption spectra (Fig. 3 and S3A†), we applied 9 GHz cw-EPR spectroscopy at liquid helium temperatures, and monitored the reaction of the $Fe^{III}L3$ porphyrin complex with m-CPBA (both in dichloromethane). The reaction of the $Fe^{III}L3$ porphyrin complex with 10-fold molar equivalents of m-CPBA was done by manual mixing and directly in a quartz EPR tube placed in a $ca.$ −100 °C bath, in order to trap the short-lived intermediates. In particular, we aimed to characterize the short-lived intermediate assigned to Compound **I**, showing an electronic absorption CT band at 705 nm and appearing within 500 ms upon a reaction of the $Fe^{III}L3$ Por complex with m-CPBA at −30 °C (Fig. 3A and S3A†). The subsequent intermediate with an electronic absorption CT band at 657 nm, and that was assigned to Compound **II**, proved to be stable for several minutes at −30 °C (Fig. S3A†). It is of note that the concentrations of the $Fe^{III}L3$ porphyrin complex used for the EPR experiments differ substantially to those used in the electronic absorption experiments, thus the yields and life time of the intermediates are not expected to be the same (see below).

The $Fe^{III}L3$ complex shows an axial EPR spectrum with observed g_{eff} values at $g_{\perp} = 6.04$ and $g_{\parallel} = 1.98$ (Fig. S5† and 7, black dotted traces), which is typical for heme iron in the ferric high-spin state. Upon reaction with m-CPBA a new and distinct EPR signal was observed: an axial and very broad (2000 G) EPR spectrum, extending between the two resonances with observed g-values of 3.80 and 1.99 (Fig. 7, green trace) that is consistent with the expected axial EPR spectrum of an exchange-coupled oxoferryl-porphyrin radical species, $[Fe^{IV}=O\,Por^{\bullet+}]$ with $g_{\perp}^{eff} = 3.80$ and $g_{\parallel}^{eff} = 1.99$, as previously reported for the porpholactone ferryl radical complexes[74] and iron porphyrins that are highly nonplanar, but not ruffled.[45,75] The fact that this new broad and axial EPR signal could only be detected at temperatures lower than 30 K (due to the line broadening effect[76]) well agrees with the expected behavior of a radical in magnetic interaction (exchange-coupling) with the ferryl moiety. Interestingly, the EPR spectrum is virtually identical, including the overall width ($ca.$ 250 G) of the resonance at $g = 3.80$ ($g_{\perp}$) and the narrow and asymmetric resonance at $g = 1.99$ ($g_{\parallel}$), to that of the previously reported $[Fe^{IV}=O\,Por^{\bullet+}]$ intermediate of nitrophorin, a heme-containing enzyme showing substantial peroxidase-like activity.[77] When thawing and incubating the EPR sample for 15 min at 20 °C, the resulting EPR spectrum

(Fig. 7, dark red trace) showed the complete disappearance of the broad axial signal of the $[Fe^{IV}=O\,Por^{\bullet+}]$ species, as expected if considering the short-lived character of this intermediate demonstrated by the stopped-flow electronic absorption experiments (Fig. S3A,† brown trace).

Compound **II**, a reaction intermediate (absorption CT band at 657 nm, Fig. S3A†) formed subsequently to the Compound **I** in the stopped-flow absorption experiments is an integer spin species ($[Fe^{IV}=O]$), thus EPR-silent. The fact that the EPR signal of the trapped $[Fe^{IV}=O\,Por^{\bullet+}]$ species does not fully account for the conversion of the ferric signal upon reaction with m-CPBA
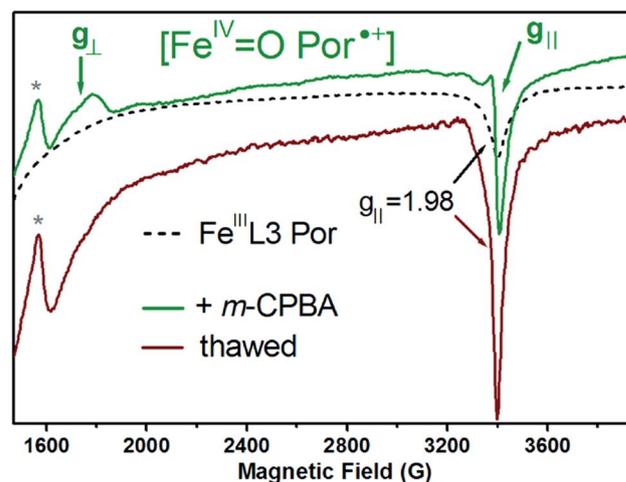

Fig. 7 The 4 K 9 GHz EPR spectra of the $[Fe^{IV}=O\,Por^{\bullet+}]$ intermediate (green trace) trapped when reacting the $Fe^{III}L3$ porphyrin complex (black dotted trace, 80 µl at 1.1 mM initial concentration) with m-chloroperbenzoic acid (20 µl at 50 mM initial concentration), both in dichloromethane and for 3 s in a cold bath (at $ca.$ −100 °C) prior to flash freezing in liquid nitrogen. The final molar excess of 10 fold was obtained for the m-CPBA oxidant. When thawing the reacted sample (green trace) for 15 min at 20 °C, spectral changes were clearly observed (dark red trace). The ferric EPR spectrum of the $Fe^{III}L3$ porphyrin complex, emulating the contribution of the non-converted complex upon reaction with m-CPBA (dotted black trace), is also plotted to better illustrate the expected difference between the $g \approx 2$ components of the ferric and the $[Fe^{IV}=O\,Por^{\bullet+}]$ intermediate. The EPR spectra (3 scans) were recorded at 4 K, 9.48 GHz frequency, 13 G modulation amplitude, 1 mW microwave power, and 100 KHz modulation frequency. The asterisk (*) shows the contribution of free iron ($g = 4.3$).

(as estimated by the decrease of the ferric EPR signal; see Fig. S5†) is fully consistent with the subsequent formation of the oxoferryl intermediate, an EPR-silent species. In addition, the higher stability of this intermediate, as shown by the stopped-flow experiments (Fig. S3A,† green trace), is consistent with the partial recovery of the ferric signal, reflected by the increase of its $g_\parallel = 1.98$ component (Fig. 8, dark red trace and Fig. S5,† dark green trace) when thawing the EPR sample for 15 min at 20 °C (see above). Further thawing and incubation of the sample (at 20 °C for 60 min) showed a small further increase in the intensity of the ferric signal (see Fig. S6†), thus confirming that the $[Fe^{IV}=O]$ species is rather stable at room temperature, as previously reported for natural peroxidases. For example, in the case of the bi-functional peroxidases KatGs, the $[Fe^{IV}=O\ Por^{\bullet+}]$ species is very short-lived while the $[Fe^{IV}=O]$ intermediate converts back to the ferric resting state only after 12 min at 20 °C, provided that all the oxidant has been used up.[78] This implies that in the $Fe^{III}L3$ porphyrin complex the hydrogen bonding stabilizes the oxoferryl intermediate.

It is of note that Dawson and coworkers, using rapid-scan stopped flow absorption spectroscopy, reported that *m*-CPBA can play both the roles of an oxidant and a substrate in the formation of the catalytic intermediates of *C. fumago* chloroperoxidase.[79] It was concluded that *m*-CPBA acts as an oxidant in the conversion of the ferric enzyme to the Compound **I** intermediate, and also as a one-electron donor (*i.e.* 'substrate') in the subsequent reductions of Compound **I** to Compound **II**, and of Compound **II** back to the ferric native enzyme.[79] In the case of the $Fe^{III}L3$ porphyrin complex reacting with *m*-CPBA, further incubation at −100 °C for 3 s showed an increase of the ferric EPR signal and no detectable change of the $[Fe^{IV}=O\ Por^{\bullet+}]$ EPR signal (Fig. S6†). This result can be rationalized as the reaction of the $[Fe^{IV}=O]$ intermediate with the remaining

m-CPBA, as in the case of chloroperoxidase. It is of note that intramolecular e$^-$ transfer reactions can readily occur at such low temperatures.[78] Taken together, these EPR experiments confirm that the $[Fe^{IV}=O\ Por^{\bullet+}]$ intermediate formed by the peroxidase-like reaction (Compound **0**–Compound **I**) of the $Fe^{III}L3$ porphyrin complex with *m*-CPBA is a short-lived species even at subzero temperatures, and that the subsequent intermediate, the $[Fe^{IV}=O]$ species (Compound **II**), formed most possibly by the reaction of the $[Fe^{IV}=O\ Por^{\bullet+}]$ intermediate with *m*-CPBA, is relatively stable at room temperature. In addition, the $[Fe^{IV}=O]$ intermediate can react slowly with *m*-CPBA as a one-electron donor, resulting in a partial cycling back to the ferric resting state.

The Compound **I** formed in most synthetic (ferric) iron porphyrin complexes readily attacks the *meso* position of the porphyrin macrocycle leading to the formation of an isoporphyrin, an intermediate leading to the eventual degradation of the iron porphyrin complex (Scheme S1†). Accordingly, the UV-vis absorption spectrum of $Fe^{III}TPP(Br)$ upon reaction with *m*-CPBA showed the appearance of the broad absorption bands at 800–900 nm (Fig. 5, red trace & S2†) consistent with the isoporphyrin species. At variance, $Fe^{III}L2(Br)$ and $Fe^{III}L3(Br)$ complexes showed very minor formation of isoporphyrin (Fig. 5A and B, violet and green traces in Fig. 5B) and converted to Compound **II** then eventually cycled back to the ferric complex, as indicated by the UV-Vis spectra and consistent with the EPR spectroscopic characterization (see above). These results suggest that not only the basic groups in $Fe^{III}L2$ and $Fe^{III}L3$ accelerate the heterolysis of the peroxide inciting the formation of Compound **I**, but also decelerate the electrophilic attack of Compound **I** on the porphyrin ring. This attribute implies that $Fe^{III}L2(Br)$ and $Fe^{III}L3(Br)$ should be able to catalyze oxidation of substrates by *m*-CPBA.

Catalytic oxidation of substrates

The reaction of $Fe^{III}L2(Br)$ and $Fe^{III}L3(Br)$ with *m*-CPBA in the presence of excess ferrocene (Fc) as an external sacrificial electron donor was monitored. The formation of a new band at 620 nm, characteristic of ferrocenium (Fc$^+$), indicates the oxidation of ferrocene by the porphyrin complexes (Fig. 8 and S7†). In the presence of excess ferrocene and *m*-CPBA, both $Fe^{III}L2$ and $Fe^{III}L3$ can catalyze its oxidation with turnover numbers (TONs) of 67 and 96, respectively, and turnover frequencies (TOFs) of 2.68 s^{-1} and 6.40 s^{-1}, respectively (Table 2). The catalytic turnover entails oxidation of two molar equivalents of ferrocene per Compound **I** species, *i.e.* Compound **I** + 2Fc → $Fe^{III}L$ + 2Fc$^+$ (Scheme 1). This result is expected, as E^o of Fc is lower than those of both Compound **I** and Compound **II**. Similar to the case of peroxidases, the organic substrate 2,4,6-tri tertiarybutyl phenol (TBPH) is oxidized to the corresponding phenoxy radical, as shown by the absorption spectra with bands at 380 nm, 400 nm and 625 nm (Fig. S7B†) and the EPR spectrum measured at 77 K shows a signal at $g = 2$ consistent with an organic radical (Fig. S8A†).[80] Both $Fe^{III}L2(Br)$ and $Fe^{III}L3(Br)$ can catalyze the oxidation of TBPH with TONs of 25 and 350, respectively, with TOFs of 1.41
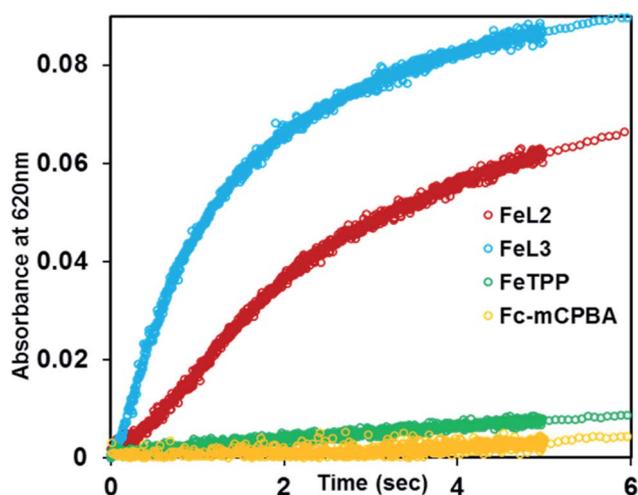

Fig. 8 The time traces in rapid scan stopped flow kinetics measurement of $Fe^{III}L2(Br)$, $Fe^{III}L3(Br)$, $Fe^{III}TPP(Br)$ complexes and the substrate (fc) with *m*-CPBA in dichloromethane at −30 °C in a cuvette of 1 cm path length with and without a catalyst for formation of ferrocenium at 620 nm by the addition of iron-porphyrins (4 μM) with *m*-CPBA (500 eq., 1 mM) and ferrocene (500 eq., 2 mM).

Table 2 Catalytic substrate oxidation

Substrate (2 mM)	$Fe^{III}L2(Br)$ (4 μM)		$Fe^{III}L3(Br)$ (4 μM)	
	TON^a	TOF^b (s^{-1})	TON^a	TOF^b (s^{-1})
Ferrocene (Fc)^c	67	2.68	96	6.40
2,4,6-Tri tertiarybutyl phenol (TBPH)^d	25	1.41	350	0.63
o-Phenylene diamine(OPD)^d	68	0.85	61	2

^{a} The maximum number of product molecules obtained from per mole of the catalyst. ^{b} TON per unit time (sec). ^{c} Stopped flow kinetics at −30 °C. ^{d} UV-visible kinetic measurements at room temperature. The other conditions are described in the Experimental section.
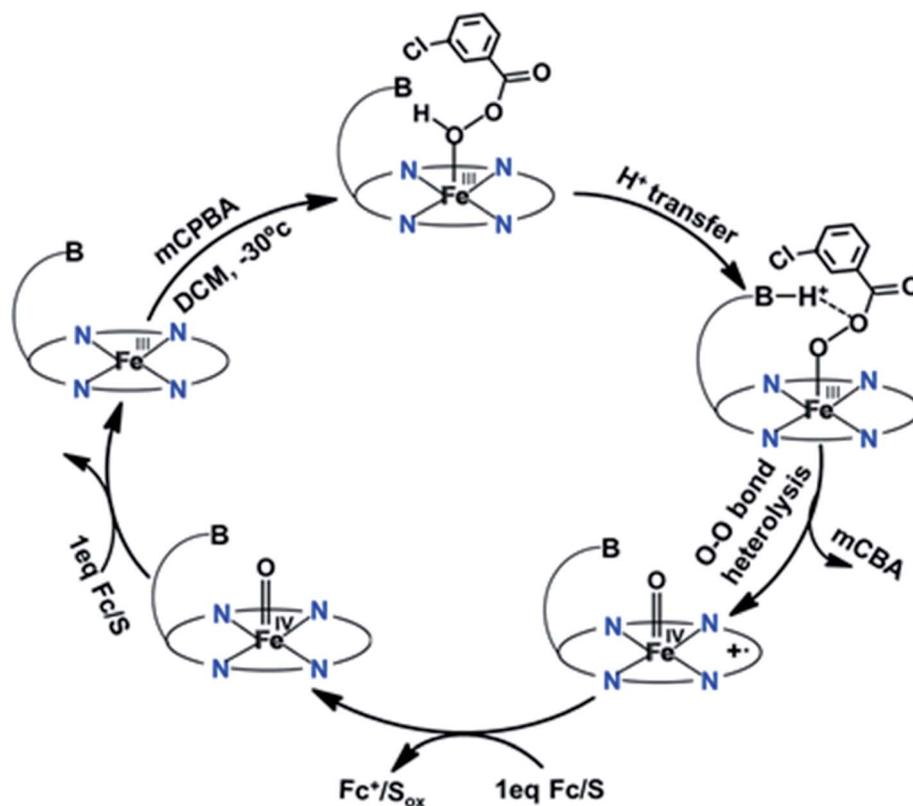
Scheme 1 Proposed mechanism of the catalytic cycle for the regeneration of high spin $Fe^{III}L2$ and $Fe^{III}L3$ via high valent intermediates starting from iron(III)-porphyrins in the presence of meta-chloroperbenzoic acid (oxidant) and ferrocene or any other one-electron donor/substrate (S) in dichloromethane at −30 °C.

s^{-1} and 0.63 s^{-1}, respectively (Table 2). Similarly, the two-electron oxidation of o-phenylene diamine (OPD) to 2,3-diaminophenazine with a characteristic absorption feature at 450 nm for these two iron porphyrins (Fig. S10†) yields TONs of 68 and 61, respectively, and the corresponding TOFs are 0.85 s^{-1} and 2 s^{-1}, respectively. Note that these are the first examples of catalytic oxidation of phenols and amines by one electron (normal peroxidase activity) using synthetic heme complexes, and using peracid as an oxidant.

DFT calculations

Having shown that facile O–O heterolysis in $Fe^{III}L2(Br)$ and $Fe^{III}L3(Br)$ allows rapid formation of Compound **I** which at its turn can oxidize ferrocene and TBPH, we performed DFT

calculations to gain theoretical insight into the effect of pendent basic groups covalently attached to iron-porphyrins in relation to such O–O bond cleavage. The structures of m-CPBA bound metal complexes are optimized in the PCM model using dichloromethane as a solvent. In general, all attempts of optimizing the peracid bound ferric state inevitably lead to spontaneous O–O heterolysis forming Compound **I** and m-chloroperbenzoic acid (Fig. 9) likely due to the acidic proton of mCPBA (pK_a = 7.5 in water). Alternatively, the electronic structure contribution of the pendent basic groups to O–O bond heterolysis can be evaluated with H_2O_2 which has a higher pK_a (11.75). Note that the use of hydrogen peroxide is more relevant to the chemistry of peroxidases. The structures with bound hydroperoxide resulting in low spin ferric porphyrins with
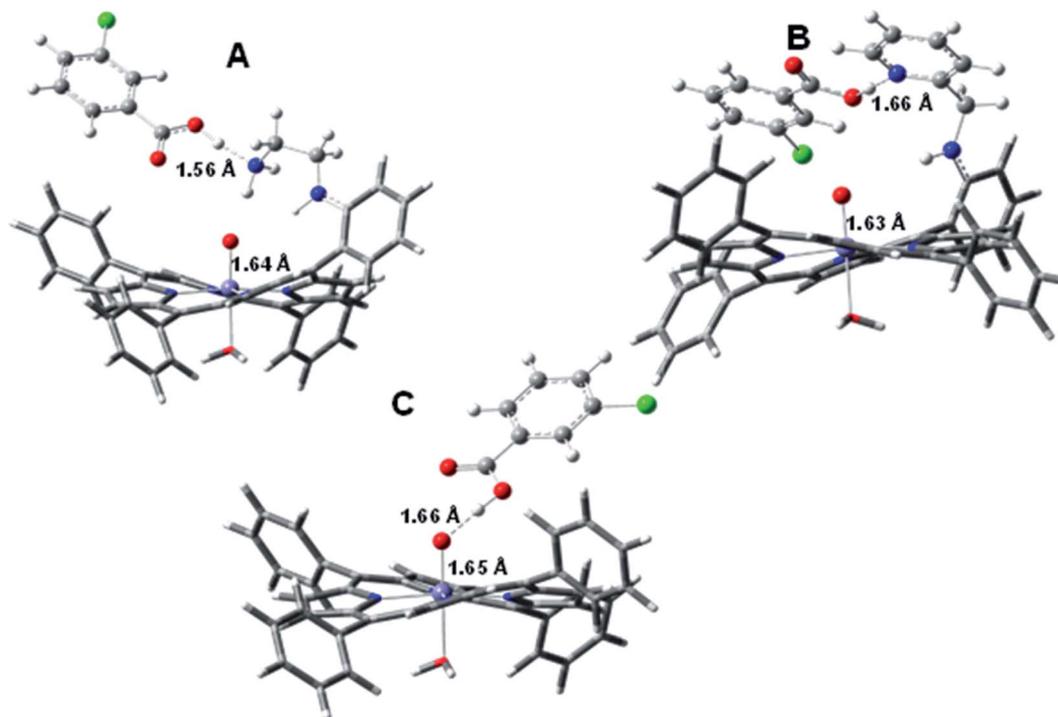
Fig. 9 Optimized structures of six coordinate low spin (A) [Fe^{III}L3-m-CPBA]H$^+$; (B) [Fe^{III}L2-m-CPBA]H$^+$; (C) [Fe^{III}TPP-m-CBPA]H$^+$ with m-CPBA and water as axial ligands and distal basic groups in the PCM model considering CH$_2$Cl$_2$ as a solvent. color codes: carbon → grey, hydrogen → white, nitrogen → blue, oxygen → red, chlorin → green and iron → bluish grey.

protonated pendent basic groups are optimized (Fig. S11†). In the case of [Fe^{III}L2-OOH]H$^+$, the –N$_1$H group and protonated pyridine (N$_2$H$^+$) act as H-bond donors to the distal oxygen atom. The optimized geometry shows that the O–O bond length for [Fe^{III}L2-OOH]H$^+$ is elongated to 1.88 Å in the protonated structure (Fig. S11†) which is much longer than those of Fe^{III}TPP-OOH (the O–O bond length is 1.46 Å) and free H$_2$O$_2$.[59]

The same trend also occurs for protonated Fe^{III}L3-OOH, where the protonated aliphatic amine group (–NH$_3^+$) elongates the O–O bond length to 1.86 Å (Fig. S11†). All these optimized geometries suggest that strong H-bond donation to the distal oxygen atom of the Fe^{III}–OOH species facilitates activation of the O–O bonds. These appended groups in the studied porphyrin complexes appear to be oriented in such a way to allow selective delivery of protons to the distal oxygen atom with simultaneous weakening of the O–O bond, both factors beneficial for heterolytic O–O bond cleavage.[59]

The substantial activation of the O–O bond of a Fe^{III}–OOH species with H-bonding by a protonated base is the root of the "pull effect" proposed in peroxidase active sites where an analogous Fe^{III}–OOH species is produced, Compound **0**.[24,81,82] The DFT calculated wave functions show that the Fe dπ character in the O–O σ* orbitals increases from 4.86% in the non H-bonded system to 36.89% and 38.69% in porphyrins having protonated OOH]H$^+$, respectively (Fig. 10).

The enhanced back-bonding is facilitated by the lowering of the O–O σ* orbital energies due to hydrogen bonding to the pendent basic groups of [Fe^{III}L3-OOH]H$^+$ and [Fe^{III}L2-OOH]H$^+$

groups (Fig. 10) which polarize the electron density of the O–O bond towards the distal OH group reducing the overlap between the two O$_{2p}$ orbitals and lowering the energy of the O–O σ* orbital. This polarization is magnified when the amines are protonated. This is evident from the calculated Mulliken charge density values on distal oxygen atoms for [Fe^{III}L3-OOH]H$^+$ (Op = −0.30 and Od = −0.60) and [Fe^{III}L2-OOH]H$^+$ (Op = −0.29 and Od = −0.61) which are more negative than those of the Fe^{III}TPP analogue (Op = −0.293 and Od = −0.383) without any hydrogen bonding residue (Fig. S12†). Thus the "pull effect" in this case may be interpreted as pulling the energy of the O–O σ* orbital down substantially by hydrogen bonding to a protonated basic residue to allow better back-bonding into the O–O σ* orbital from the filled Fe dπ orbital of the metal. The O$_{2p}$ coefficient increases from 3.62% in Fe^{III}TPP-OOH to 18.05% in [Fe^{III}L3-OOH]H$^+$ and 17.55% in [Fe^{III}L2-OOH]H$^+$ in the dπ orbital signifying increased covalent donation from the proximal oxygen to the empty Fe dπ orbital *i.e.* strong π bonding (Fig. 10). A similar increase in σ covalency is observed in the d$_{z2}$ orbital. These are consistent with the shortening of the Fe–O bond upon elongation of the O–O bond taking the reactant Fe^{III}–OOH to the product [Fe(ɪᴠ) ═O Por$^{•+}$].

In nature, the alternative mechanism of activating a Fe^{III}–OOH used in Cyt P450 and CPO is the "push effect" of an axial thiolate ligand. The anionic thiolate ligand enhances the electron density of its trans axial ligand increasing the basicity. This enhanced pK$_a$ (~12) leads to a protonated Compound **II** in Cyt p450/CPO when Compound **II** is deprotonated in peroxidases/
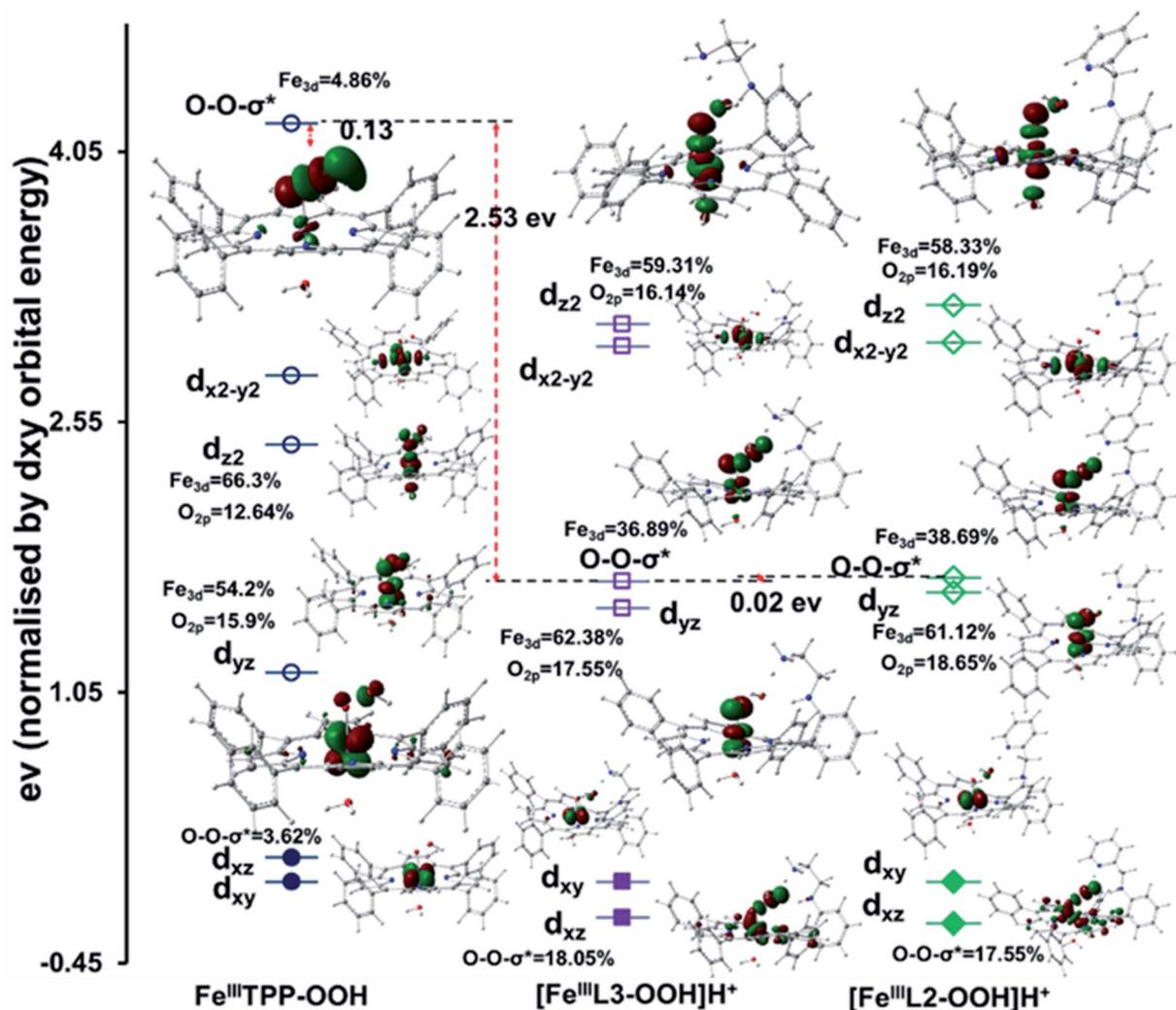
Fig. 10 Calculated (BP86) ground state MO diagrams of Fe(III)TPP-OOH (no H-bonding residue), [Fe(III)L3-OOH]H⁺) and [Fe(III)L2-OOH]H⁺ (protonated H-bonding residue). The relative energies are normalized with respect to the non-bonding d_{xy} orbital. Only β orbitals are shown. The orbital contributions of the occupied d_{xz} orbital and the unoccupied O−O σ* orbital are shown. The contributions of d_{z^2} and the d_{yx} orbitals of the Fe that σ and π bonds, respectively, to the hydroperoxide are also shown. The non-bonding d_{xy} and the $d_{x^2-y^2}$ are not shown for clarity.

myoglobin with a pK_a of around 3.[83,84] DFT calculations on a hypothetical thiolate bound Fe^{III}TPP-OOH species show a O–O bond length of 1.46 Å which is shorter than that of [Fe^{III}L2-OOH]H⁺ with a protonated pendent base (1.88 Å) and the Fe–O

bond length of thiolate bound Fe^{III}TPP-OOH is calculated to be 1.85 Å which is shorter than that of [Fe^{III}L2-OOH]H⁺ (Fig. S11†). The Mulliken charge on the hydroperoxide unit of the thiolate bound Fe^{III}TPP-OOH species is calculated to be Op = −0.362
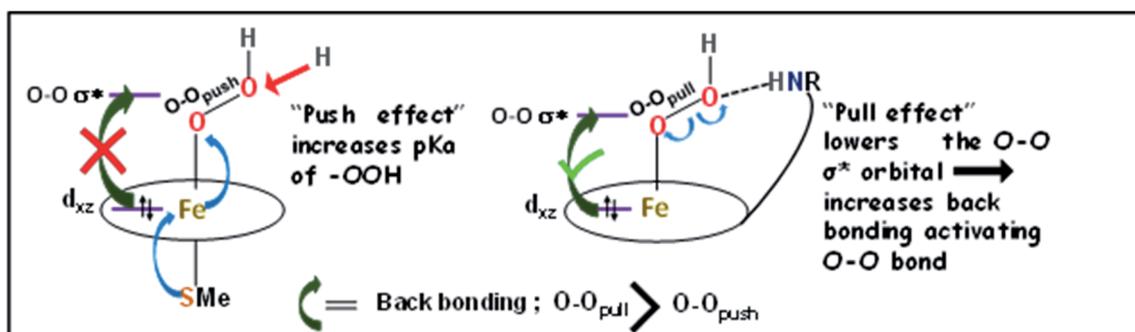

Fig. 11 Schematic representation of O−O bond activation by the "push effect" and the "pull effect".

and Od = −0.422. The negative charge of the distal oxygen atom of the bound hydroperoxide is substantially more negative than a $Fe^{III}TPP$-OOH without axial thiolate (Op = −0.293, Od = −0.383) (Fig. S12†). The MO diagram of the thiolate bound $Fe^{III}TPP$-OOH shows much less electron donation by the bound –OOH to the Fe dσ and dπ orbitals consistent with greater anionic charge on the bound hydroperoxide relative to $Fe^{III}TPP$-OOH. There is very little Fe_{3d} character in O–O σ* suggesting the lack of back-bonding from the filled Fe_{3d} consistent with the short O–O distance (Fig. S13†). Thus the "push effect" of the thiolate is limited to push electron density to the bound –OOH ligand increasing its basicity causing its protonation at physiological pH (Fig. 11). Once protonated, the resulting Fe^{III}–OOH_2^+ species will have a very weak O–O bond which would cleave almost spontaneously. Alternatively, the "pull effect" of the pendent basic group results from polarization of the electron density of the peroxide resulting in lowering the O–O σ* energy (Fig. 11) which allows greater back-bonding into O–O σ* from the filled 3d orbitals of the iron due to better energy match, and thus weakening of the O–O σ bond activates the O–O bond for cleavage.

Conclusion

Inclusion of pendent basic groups in iron porphyrins, mimicking the 2nd sphere interactions present in the distal site of HRP, enables facile O–O bond heterolysis of peracids having barriers lower than naturally occurring enzymes. The Compound **I** generated by these iron porphyrin complexes with 2nd sphere coordination is capable of oxidizing two equivalents of substrates (both organic and inorganic) thus making them functional models of natural peroxidases. The introduced basic groups, mimicking the His–Arg base pair in the active site of horseradish peroxidase, not only enable facile heterolysis but also stabilize the Compound **I** and Compound **II** intermediates. More importantly, electrophilic attack on the porphyrin macrocycle is prevented and such intermediates effectively oxidize organic and inorganic substrates, using an outer-sphere electron transfer mechanism. Accordingly, these synthetic complexes act as efficient catalysts with reasonable TONs and TOFs. Investigations are underway to understand how the hydrogen bonding tunes the reactivity of the high valent oxoferryl species from electrophilic inner-sphere oxidation (monooxygenase-like) to outer-sphere electron transfer (peroxidase-like).

Experimental procedures

Instrumentation

All UV-visible absorption spectra were recorded on an Agilent 8453 diode array spectrophotometer in a cuvette of 1 cm path length at room temperature unless otherwise mentioned. Rapid mixing stopped flow kinetics were performed on a SFM 4000 spectrophotometer (halogen-deuterium lamp as the light source) equipped with a low temperature chamber. The 4 K 9 GHz EPR spectra were recorded on a Bruker EleXsys E500 spectrometer equipped with a standard Bruker ER4102 X-band resonator and a liquid helium cryostat (Oxford Instruments, ESR 900). EPR quartz tubes of 4 mm external diameter were used. A JEOL FA200 spectrometer was used for the measurements at 77 K.

Materials

All reagents were of the highest grade commercially available and were used without further purification. The iron-porphyrins ($Fe^{III}L2(Br)$, $Fe^{III}L3(Br)$ and $Fe^{III}TPP(Br)$) studied here were synthesized according to previously reported procedures.[59] 3-Chloroperoxybenzoic acid (*m*-CPBA) was purchased from Aldrich (77%) and purified by washing with pH 7.40 phosphate buffer and recrystallized from pentane to remove 3-chlorobenzoic acid. Purity (>95%) was determined by ^{1}H NMR. Solvents were purchased from RANKEM with HPLC grade for spectroscopic purpose. 2,4,6-Tritertiary butyl phenol (TBPH) and ferrocene (Fc) were also purchased from Sigma-Aldrich.

Synthesis

(1a) Mono benzyl substituted monoamino porphyrin (MPh). The synthetic strategy utilized *o*-aminophenyl-tris(phenyl)-porphyrin (MAPP) as a starting material.[85] To a 20 ml solvent mixture of THF–acetonitrile (1 : 3), MAPP (50 mg, 0.079 mmol) was added. After adding benzaldehyde (30 μl, 0.316 mmol) and trifluoroacetic acid (28 μl, 0.371 mmol) to the solution, the solution turned green. After 2 h, 5 equivalent of NaBH₄ (16 mg, 0.417 mmol) was added to the reaction and was further stirred for 12 h. The colour again changed to reddish brown. The solvent was removed through a rotary evaporator and the compound was extracted with dichloromethane. The organic layer was dried with Na₂SO₄ and the solvent was evaporated to isolate the compound. Then the desired compound was eluted with a 50% DCM–hexane mixture through column chromatography using neutral alumina and purple coloured solid was isolated (Mph, Scheme S2†). Yield: (45 mg, 80%); ^{1}H NMR (500 MHz,CDCl₃, 25 °C): δ, ppm = 9.03 (m, 8H), 8.30 (d, 6H), 7.95 (d, 1H), 7.83 (m, 9H), 7.66 (t, 1H), 7.13 (m, 7H), 7.05 (m, 2H), 4.55 (d, 2H), 3.88(t, NH), −2.62 (s, 2H); UV-Vis (CH₂Cl₂): λ_{max} = 418 nm, 516 nm, 551 nm, 591 nm, 651 nm; ESI-MS (positive ion mode in ACN): *m/z* (%) = 720.29 (100) [MPh]H⁺.

(1b) Mono benzyl substituted monoamino iron porphyrin [$Fe^{III}MPh(Br)$]. The ligand (50 mg, 0.069 mmol) was dissolved in dry degassed THF and about 18 μl of collidine was added to it and stirred for 5 minutes. Then Fe^{II}Br₂ (60 mg, 0.276 mmol) was also added and stirred, overnight. After the completion of the reaction the solvent was removed and the reaction mixture was worked up with DCM after treating with dil. HCl to remove excess FeBr₂. The organic layer was dried over anhydrous Na₂SO₄ and evaporated using a rotary evaporator. The reddish brown colored solid was isolated ($Fe^{III}MPh(Br)$, Scheme S2†). Yield: (51 mg, 95%); elemental analysis calcd (%) for [$Fe^{III}L2$]Br (C₅₁H₃₅BrFeN₅·C₆H₁₄): C 72.85, H 5.26, N 7.45; found: C 73.46, H 5.34, N 7.89; ^{1}H NMR (500 MHz, CDCl₃, 25 °C): δ, ppm = 79.70 (pyrrolic protons), 12–14 (meta hydrogens of phenyl rings of the porphyrin); UV-Vis (CH₂Cl₂): λ_{max} = 417 nm, 510 nm, 584 nm,

660 nm and 696 nm. ESI-MS (positive ion mode in ACN): m/z (%) = 773.23 (100) [Fe^{III}MPh].

(2a) UV-visible absorption kinetics of substrate oxidation. In a cuvette containing 2 ml dichloromethane, iron porphyrin (8 μl, 1 mM), m-CPBA (40 μl, 50 mM) and TBPH (40 μl, 100 mM) were added resulting in a final ratio of the mixture as a catalyst: m-CPBA : TBPH = 1 : 250 : 500. The kinetics were recorded at room temperature and using a time interval of 0.5 s. Oxidation of TBPH to a 2,4,6-tri tertiary butyl phenoxyl (TBP) radical was monitored using the time traces of the characteristic absorption bands at 380 nm, 400 nm and 635 nm. Similar conditions were applied for OPD oxidation to the corresponding 2,3-diaminophenazine formation with an absorption feature at 450 nm.

(2b) Stopped flow kinetics. In order to measure the rapid kinetics for Compound **I** formation, a cuvette of 1 cm path length was used. One gastight syringe was filled with the porphyrin compound (50 μM, 3 ml) and the other with m-CPBA (200 μM, 5 ml) in dichloromethane. Then the solutions were loaded into the spectrophotometer and triggered by simultaneous injection of each solution according to the required ratio of the compound and oxidant. The solutions were cooled to −30 °C prior to mixing and maintained in a chilled isopentane bath throughout the reaction.

The reactions with ferrocene as a substrate were very rapid at room temperature and thus were performed in the stopped-flow set-up immersed in a cold bath (−30 °C). In a typical experiment, three syringes were filled with ferrocene (2 mM, 3 ml), m-CPBA (1 mM, 5 ml) and iron porphyrin (4 μM, 2 ml), respectively, and volumes of these were injected to achieve a final concentration ratio of 1 : 250 : 500 for iron porphyrins : m-CPBA : ferrocene of the mixture.

(2c) Fitting of the kinetic data

$$y = y_0 + A_0 \exp(-kt)$$

or,

$$\log A_0 = kt + \log(y - y_0)$$

The above first order monophasic equation was used to fit the kinetics data and thus obtained the first order rate constants of initial formation and decay from the slope of the linear fit in the $\log A_0$ vs. time trace plot.

(2d) TON calculations. TONs for substrate oxidation have been calculated with iron porphyrins (0.2 mol%) and oxidant like m-CPBA (substrate : m-CPBA : catalyst = 1 : 250 : 500) from the ratio of the oxidized product concentration to the initial catalyst concentration. For this purpose, we have determined the product concentration (c) from measured absorbance (A) and known molar extinction coefficient (ε) using equation $A = \varepsilon \times c \times l$ (where, the path length of cuvette l = 1 cm).

For ferrocenium hexafluorophosphate, the molar extinction coefficient (ε) value from the slope of absorbance vs. concentration dependence plot (Fig. S9†) was calculated to be 350.34 M^{-1} cm^{-1}. The ε values 404 M^{-1} cm^{-1} and 11.1 mM^{-1} cm^{-1} for TBPH and OPD, respectively, were obtained from an earlier report.[80,86] TON is the number of substrate molecules oxidized into the product by per mole of the catalyst. TOFs have been calculated by dividing the TON with the time required for maximum product conversion estimated at the highest absorbance (Table 2). The TOF thus obtained represents an average rate over the entire duration of the reaction and not an initial rate.

(3) EPR spectroscopy and sample preparation. The EPR samples for the 4 K measurements were prepared by manual mixing of 80 μl of the Fe^{III}L3 porphyrin complex dissolved in dichloromethane (initial concentration of 1.1 mM) with 20 μl of m-chloroperbenzoic acid (initial concentration of 50 mM), thus obtaining a final molar excess of 10 fold for the m-CPBA oxidant. The manual mixing of the complex with the oxidant was done directly in the 4 mm-EPR tube, kept in a cold bath of 2-methylTHF/liq N$_2$ (ca. −100 °C). The mixing time was 3 s, prior to flash freezing the sample in liquid nitrogen. It is of note that longer mixing times and/or higher temperatures resulted in a faster conversion of the [Fe^{IV}=O Por$^{•+}$] to the [Fe^{IV}=O] intermediate.

For the 77 K EPR measurement of the TBP radicals, samples were prepared in an EPR quartz tube using 80 μl of 2 mM TBPH, 10 μl of 10 mM m-CPBA and 10 μl of 44 μM FeL2/FeL3, so that the concentration ratio of the final resulting sample was 1 : 250 : 500 for iron porphyrins: m-CPBA : TBPH. The reaction mixture was kept in a −80 °C bath for 1 min before flash freezing in liquid nitrogen.

(4) DFT calculations. The geometry of all compounds was optimized in the gradient corrected BP86 Functional in unrestricted formalism using Gaussian 03 version C03. For hydroperoxide models, Fe, N and O atoms were optimised using the 6-311G(d) basis set and 6-31G(d) for all other atoms. For m-CPBA bound models, the Fe, N and O atoms were optimized using the 6-311G(d) basis set and the 6-31G(d) basis set for all other atoms in a polarizable continuum model with dichloromethane.[87] The fully optimized structure is confirmed by calculating their frequency using the same basis set to ensure no imaginary mode is present for all these compounds. The final energy calculations were performed using the 6-311+G(d) basis set on all atoms in the PCM model using dichloromethane as a solvent and a convergence criterion of 10^{-10} Hartree.[88–90]

Conflicts of interest

There are no conflicts of interest.

Acknowledgements

References

1 S. Chatterjee, K. Sengupta, B. Mondal, S. Dey and A. Dey, *Acc. Chem. Res.*, 2017, **50**, 1744–1753.

2 S. M. Adam, I. Garcia-Bosch, A. W. Schaefer, S. K. Sharma, M. A. Siegler, E. I. Solomon and K. D. Karlin, *J. Am. Chem. Soc.*, 2017, **139**, 472–481.

3 M. Bhadra, J. Y. C. Lee, R. E. Cowley, S. Kim, M. A. Siegler, E. I. Solomon and K. D. Karlin, *J. Am. Chem. Soc.*, 2018, **140**, 9042–9045.

4 R. Cao, C. Saracini, J. W. Ginsbach, M. T. Kieber-Emmons, M. A. Siegler, E. I. Solomon, S. Fukuzumi and K. D. Karlin, *J. Am. Chem. Soc.*, 2016, **138**, 7055–7066.

5 K. Cheaib, M. Q. E. Mubarak, K. Sénéchal-David, C. Herrero, R. Guillot, M. Clémancey, J.-M. Latour, S. P. de Visser, J.-P. Mahy, F. Banse and F. Avenier, *Angew. Chem.*, 2019, **131**, 864–868.

6 A. W. Schaefer, M. T. Kieber-Emmons, S. M. Adam, K. D. Karlin and E. I. Solomon, *J. Am. Chem. Soc.*, 2017, **139**, 7958–7973.

7 L. Nurdin, D. M. Spasyuk, L. Fairburn, W. E. Piers and L. Maron, *J. Am. Chem. Soc.*, 2018, **140**, 16094–16105.

8 T. L. Poulos, *Chem. Rev.*, 2014, **114**, 3919–3962.

9 A. Díaz, P. C. Loewen, I. Fita and X. Carpena, *Arch. Biochem. Biophys.*, 2012, **525**, 102–110.

10 A. Ivancich and P. C. Loewen, Electron Transfer in Catalases and Catalase-Peroxidases, *Encyclopedia of Biophysics, European Biophysical Societies' Association (EBSA) 2018*, ed. G. Roberts and Watts A., Springer, Berlin, Heidelberg, 2018, DOI: 10.1007/978-3-642-35943-9_51-1.

11 E. J. Mueller, P. J. Loida and S. G. Sligar, in *Cytochrome P450: Structure, Mechanism, and Biochemistry*, ed. P. R. O. de Montellano, Springer US, Boston, MA, 1995, pp. 83–124, DOI: 10.1007/978-1-4757-2391-5_3.

12 A. W. Munro, K. J. McLean, J. L. Grant and T. M. Makris, *Biochem. Soc. Trans.*, 2018, **46**, 183–196.

13 F. R. S. D. Keilin and T. Mann, *Proc. R. Soc. London, Ser. B*, 1937, **122**, 119.

14 F. L. Muller, M. S. Lustgarten, Y. Jang, A. Richardson and H. Van Remmen, *Free Radicals Biol. Med.*, 2007, **43**, 477–503.

15 M. Zamocky, C. Jakopitsch, P. G. Furtmüller, C. Dunand and C. Obinger, *Proteins: Struct., Funct., Bioinf.*, 2008, **72**, 589–605.

16 S. Ghasempur, S.-F. Torabi, S.-O. Ranaei-Siadat, M. Jalali-Heravi, N. Ghaemi and K. Khajeh, *Environ. Sci. Technol.*, 2007, **41**, 7073–7079.

17 O. Kirk, T. V. Borchert and C. C. Fuglsang, *Curr. Opin. Biotechnol.*, 2002, **13**, 345–351.

18 Y. Watanabe, H. Nakajima and T. Ueno, *Acc. Chem. Res.*, 2007, **40**, 554–562.

19 L. A. Blumenfeld, R. M. Davydov, N. S. Fel, S. N. Magonov and R. O. Vilu, *FEBS Lett.*, 1974, **45**, 256–258.

20 T. L. Poulos and J. Kraut, *J. Biol. Chem.*, 1980, **255**, 8199–8205.

21 D. Dolphin, A. Forman, D. C. Borg, J. Fajer and R. H. Felton, *Proc. Natl. Acad. Sci.*, 1971, **68**, 614–618.

22 T. Matsui, S.-i. Ozaki, E. Liong, G. N. Phillips and Y. Watanabe, *J. Biol. Chem.*, 1999, **274**, 2838–2844.

23 A. N. P. Hiner, E. L. Raven, R. N. F. Thorneley, F. García-Cánovas and J. N. Rodríguez-López, *J. Inorg. Biochem.*, 2002, **91**, 27–34.

24 S.-i. Ozaki, M. P. Roach, T. Matsui and Y. Watanabe, *Acc. Chem. Res.*, 2001, **34**, 818–825.

25 E. Derat and S. Shaik, *J. Phys. Chem. B*, 2006, **110**, 10526–10533.

26 J. N. Rodríguez-López, D. J. Lowe, J. Hernández-Ruiz, A. N. P. Hiner, F. García-Cánovas and R. N. F. Thorneley, *J. Am. Chem. Soc.*, 2001, **123**, 11838–11847.

27 J. E. Erman, L. B. Vitello, M. A. Miller, A. Shaw, K. A. Brown and J. Kraut, *Biochemistry*, 1993, **32**, 9798–9806.

28 G. I. Berglund, G. H. Carlsson, A. T. Smith, H. Szöke, A. Henriksen and J. Hajdu, *Nature*, 2002, **417**, 463.

29 B. D. Howes, J. N. Rodriguez-Lopez, A. T. Smith and G. Smulevich, *Biochemistry*, 1997, **36**, 1532–1543.

30 T. L. Poulos, S. T. Freer, R. A. Alden, S. L. Edwards, U. Skogland, K. Takio, B. Eriksson, N. Xuong, T. Yonetani and J. Kraut, *J. Biol. Chem.*, 1980, **255**, 575–580.

31 I. Fita and M. G. Rossmann, *J. Mol. Biol.*, 1985, **185**, 21–37.

32 M. Sundaramoorthy, J. Terner and T. L. Poulos, *Structure*, 1995, **3**, 1367–1378.

33 J. N. Rodríguez-López, M. A. Gilabert, J. Tudela, R. N. F. Thorneley and F. García-Cánovas, *Biochemistry*, 2000, **39**, 13201–13209.

34 S. Bhakta, A. Nayek, B. Roy and A. Dey, *Inorg. Chem.*, 2019, **58**, 2954–2964.

35 J. N. Rodriguez-Lopez, A. T. Smith and R. N. F. Thorneley, *J. Biol. Chem.*, 1996, **271**, 4023–4030.

36 R. Nakajima and I. Yamazaki, *J. Biol. Chem.*, 1980, **255**, 2067–2071.

37 S. Marklund, *Arch. Biochem. Biophys.*, 1973, **154**, 614–622.

38 J. H. Dawson, *Science*, 1988, **240**, 433.

39 Y. Watanabe and T. Ueno, *Bull. Chem. Soc. Jpn.*, 2003, **76**, 1309–1322.

40 S. R. Bell and J. T. Groves, *J. Am. Chem. Soc.*, 2009, **131**, 9640–9641.

41 N. Jin, D. E. Lahaye and J. T. Groves, *Inorg. Chem.*, 2010, **49**, 11516–11524.

42 K. Yamaguchi, Y. Watanabe and I. Morishima, *J. Am. Chem. Soc.*, 1993, **115**, 4058–4065.

43 J. T. Groves and Y. Watanabe, *J. Am. Chem. Soc.*, 1988, **110**, 8443–8452.

44 J. T. Groves and Y. Watanabe, *J. Am. Chem. Soc.*, 1986, **108**, 7834–7836.

45 H. Fujii, T. Yoshimura and H. Kamada, *Inorg. Chem.*, 1996, **35**, 2373–2377.

46 J. D. Soper, S. V. Kryatov, E. V. Rybak-Akimova and D. G. Nocera, *J. Am. Chem. Soc.*, 2007, **129**, 5069–5075.

47 C. J. Chang, L. L. Chng and D. G. Nocera, *J. Am. Chem. Soc.*, 2003, **125**, 1866–1876.

48 F. Hollmann, P.-C. Lin, B. Witholt and A. Schmid, *J. Am. Chem. Soc.*, 2003, **125**, 8209–8217.

49 S. Shaik, S. Cohen, Y. Wang, H. Chen, D. Kumar and W. Thiel, *Chem. Rev.*, 2010, **110**, 949–1017.

50 C. J. Thibodeaux, W.-c. Chang and H.-w. Liu, *Chem. Rev.*, 2012, **112**, 1681–1709.

51 H. B. Dunford and B. B. Hasinoff, *Biochemistry*, 1970, **9**, 4930–4939.

52 E. G. Hrycay and S. M. Bandiera, in *Monooxygenase, Peroxidase and Peroxygenase Properties and Mechanisms of Cytochrome P450*, ed. E. G. Hrycay and S. M. Bandiera, Springer International Publishing, Cham, 2015, pp. 1–61, DOI: 10.1007/978-3-319-16009-2_1.

53 M. I. Savenkova, J. M. Kuo and P. R. Ortiz de Montellano, *Biochemistry*, 1998, **37**, 10828–10836.

54 J. T. Groves and T. E. Nemo, *J. Am. Chem. Soc.*, 1983, **105**, 5786–5791.

55 B. Meunier, *Chem. Rev.*, 1992, **92**, 1411–1456.

56 X. Huang and J. T. Groves, *Chem. Rev.*, 2018, **118**, 2491–2553.

57 T. G. Traylor, W. A. Lee and D. V. Stynes, *J. Am. Chem. Soc.*, 1984, **106**, 755–764.

58 T. G. Traylor and R. Popovitz-Biro, *J. Am. Chem. Soc.*, 1988, **110**, 239–243.

59 S. Bhunia, A. Rana, P. Roy, D. J. Martin, M. L. Pegis, B. Roy and A. Dey, *J. Am. Chem. Soc.*, 2018, **140**, 9444–9457.

60 I. Kaljurand, T. Rodima, I. Leito, I. A. Koppel and R. Schwesinger, *J. Org. Chem.*, 2000, **65**, 6202–6208.

61 H. Fujii, *J. Am. Chem. Soc.*, 1993, **115**, 4641–4648.

62 I. Garcia-Bosch, S. K. Sharma and K. D. Karlin, *J. Am. Chem. Soc.*, 2013, **135**, 16248–16251.

63 S. Yokota and H. Fujii, *J. Am. Chem. Soc.*, 2018, **140**, 5127–5137.

64 W. D. Hewson and L. P. Hager, *J. Biol. Chem.*, 1979, **254**, 3182–3186.

65 M. M. Palcic, R. Rutter, T. Araiso, L. P. Hager and H. B. Dunford, *Biochem. Biophys. Res. Commun.*, 1980, **94**, 1123–1127.

66 Z. Pan and M. Newcomb, *Inorg. Chem. Commun.*, 2011, **14**, 968–970.

67 Z. Pan and M. Newcomb, *Inorg. Chem.*, 2007, **46**, 6767–6774.

68 X. Lu, X.-X. Li, M. S. Seo, Y.-M. Lee, M. Clémancey, P. Maldivi, J.-M. Latour, R. Sarangi, S. Fukuzumi and W. Nam, *J. Am. Chem. Soc.*, 2019, **141**, 80–83.

69 Z. Cong, T. Kurahashi and H. Fujii, *J. Am. Chem. Soc.*, 2012, **134**, 4469–4472.

70 D. M. Davies, P. Jones and D. Mantle, *Biochem. J.*, 1976, **157**, 247–253.

71 S. L. Newmyer and P. R. O. de Montellano, *J. Biol. Chem.*, 1995, **270**, 19430–19438.

72 T. L. Poulos, *Arch. Biochem. Biophys.*, 2010, **500**, 3–12.

73 M. I. Savenkova, S. L. Newmyer and P. R. Ortiz de Montellano, *J. Biol. Chem.*, 1996, **271**, 24598–24603.

74 K. Jayaraj, A. Gold, R. N. Austin, L. M. Ball, J. Terner, D. Mandon, R. Weiss, J. Fischer, A. DeCian, E. Bill, M. Müther, V. Schünemann and A. X. Trautwein, *Inorg. Chem.*, 1997, **36**, 4555–4566.

75 K. Ayougou, D. Mandon, J. Fischer, R. Weiss, M. Müther, V. Schünemann, A. X. Trautwein, E. Bill, J. Terner, K. Jayaraj, A. Gold and R. N. Austin, *Chem.–Eur. J.*, 1996, **2**, 1159–1163.

76 J. T. Colvin, R. Rutter, H. J. Stapleton and L. P. Hager, *Biophys. J.*, 1983, **41**, 105–108.

77 R. Singh, R. E. Berry, F. Yang, H. Zhang, F. A. Walker and A. Ivancich, *Biochemistry*, 2010, **49**, 8857–8872.

78 A. Ivancich, L. J. Donald, J. Villanueva, B. Wiseman, I. Fita and P. C. Loewen, *Biochemistry*, 2013, **52**, 7271–7282.

79 D. P. Collins, I. S. Isaac, E. D. Coulter, P. W. Hager, D. P. Ballou and J. H. Dawson, *J. Porphyrins Phthalocyanines*, 2013, **17**, 63–72.

80 E. R. Altwicker, *Chem. Rev.*, 1967, **67**, 475–531.

81 E. Derat, S. Shaik, C. Rovira, P. Vidossich and M. Alfonso-Prieto, *J. Am. Chem. Soc.*, 2007, **129**, 6346–6347.

82 H. K. Baek and H. E. Van Wart, *Biochemistry*, 1989, **28**, 5714–5719.

83 K. L. Stone, R. K. Behan and M. T. Green, *Proc. Natl. Acad. Sci.*, 2006, **103**, 12307–12310.

84 T. H. Yosca, R. K. Behan, C. M. Krest, E. L. Onderko, M. C. Langston and M. T. Green, *J. Am. Chem. Soc.*, 2014, **136**, 9124–9131.

85 J. P. Collman, J. I. Brauman, K. M. Doxsee, T. R. Halbert, E. Bunnenberg, R. E. Linder, G. N. LaMar, J. Del Gaudio, G. Lang and K. Spartalian, *J. Am. Chem. Soc.*, 1980, **102**, 4182–4192.

86 O. V. Ignatenko, I. Gazaryan, E. A. Mareeva, T. A. Chubar, V. A. Fechina, P. Savitsky, A. M Rojkova and V. Tishkov, *Catalytic Properties of Tryptophanless Recombinant Horseradish Peroxidase*, 2000.

87 J. P. Perdew, *Phys. Rev. B*, 1986, **33**, 8822–8824.

88 S. Miertuš, E. Scrocco and J. Tomasi, *Chem. Phys.*, 1981, **55**, 117–129.

89 L. Noodleman and W.-G. Han, *JBIC, J. Biol. Inorg. Chem.*, 2006, **11**, 674–694.

90 M. G. Ullmann, L. Noodleman and D. A. Case, *JBIC, J. Biol. Inorg. Chem.*, 2002, **7**, 632–639.